Supporting Information

Boura et al. 10.1073/pnas.1101763108

SI Text

SI Analysis. ***Dynamics of single-molecule FRET.*** To evaluate the contribution of dynamics to the width of the measured FRET efficiency histogram, we used the maximum likelihood method of Gopich and Szabo (1). In this method, the optimal values of two mean FRET efficiencies and two rate coefficients for transition between the two states were determined that maximized the likelihood of observing the photon trajectories, consisting of a color for each photon and the interval between it and the preceding photon (2, 3). The FRET efficiencies determined by this method are 0.53 and 0.85 for the open and closed forms, respectively, which are in excellent agreement with the mean FRET efficiencies calculated for the model structures of 0.63 and 0.85, corresponding to differences in mean distances of approximately 0.3 nm and approximately 0.2 nm, respectively. The fraction of the closed form is 0.46, which is also close to the modeling result of 0.50. The sum of the two rate coefficients k is 1.04 ms^{-1}, which is similar to the 2-ms bin time as expected from the broadening. The recolored histogram using these parameters reproduces the experimental results much better than the static model as shown in Fig. S3*A*. However, this possibility of two-state conformational dynamics is ruled out by the inconsistency in the bin time dependence. Fig. S3 shows the histograms constructed with bin times of 0.5 ms (Fig. S3*C*), 1.0 ms (Fig. S3*B*), and 2 ms (Fig. S3*A*) while keeping the photon threshold at 50. If dynamics were responsible for the broad experimental histogram constructed from 2-ms bins, then the histogram should change with bin size and show signs of two distinct peaks emerging as the bin size decreases. No such difference in the measured histograms is observed, suggesting that dynamics are not responsible for the broad measured histogram. We should mention, however, that conformational dynamics is not completely ruled out, and the model structures might be even more consistent with the measured histograms with a much more complex model in which there are dynamics among all six clusters (4.)

Fluorescence anisotropy. The second possibility for the difference in measured and predicted smFRET histograms is slow orientational averaging of dyes. Most FRET measurements assume there is an isotropic distribution of donor and acceptor dye transition dipoles that reorient faster than the fluorescence lifetimes. This fast averaging results in the orientational factor $\kappa^2 = 2/3$. If the dye reorientational times are longer than the fluorescence lifetimes, caused, for example, by transient sticking of dyes to the protein, but shorter than the time interval between detected photons (approximately 20 μs), or if the space accessible to the dyes is restricted, κ^2 will not be 2/3. In these cases there will be no broadening in excess of the shot noise. However, if the dye reorientational time is comparable to or longer than the interphoton time, not only is $\kappa^2 \neq 2/3$, but there will be broadening of the FRET efficiency peaks in excess of the contribution from shot noise (5).

To test for slow orientational averaging of dyes, we measured the steady-state polarization anisotropy (r_a) defined as

$$r_a = \frac{Gn_{||} - n_{\perp}}{Gn_{||}(1 - 3k_2) + n_{\perp}(2 - 3k_1)}. \qquad [S1]$$

Here, $n_{||}$ and $n_{\perp}$ are the number of photons detected in parallel and perpendicular polarization channels for a given bin, $k_1 (= 0.11)$ and $k_2 (= 0.20)$ are objective calibration parameters, and $G (= 0.78\,(\text{donor}), 0.92\,(\text{acceptor}))$ is the correction factor for the detection efficiency of the two polarization channels (6, 7). The anisotropy of a freely rotating donor dye is given by

$$r_a = \frac{3\cos^2\theta - 1}{5(1 + \tau_D/\tau_c)}, \qquad [S2]$$

where θ is the angle between absorption and emission dipoles, assumed to be zero, τ_D is the donor lifetime, and τ_c is the reorientational correlation time for the transition dipole moments of the dyes. Therefore, the anisotropy values can be different depending on the FRET efficiency with different τ_D even though τ_c is the same. The anisotropy values determined from the photons in bins at different FRET efficiency ranges are compared in Table S3.

Because the acceptor dye was not excited directly by a laser and the excitation energy was transferred from the donor, r_A is not the exact anisotropy defined in Eq. **S1**. However, the value is small, suggesting fast orientational averaging of the acceptor.

SI Methods. ***Protein expression and purification.*** Wild-type yeast ESCRT-I complex and all mutants were expressed and purified as described previously (8). Double cysteine mutants were prepared by QuikChange site-directed mutagenesis kit (Stratgene) in the background of a construct in which all naturally occurring Cys had been mutated to Ala ($Mvb12^{C48A/C54A/C61A}$, $Vps37^{C123A}$, $Vps28^{C101A}$, $Vps23^{C133A,C344A}$). Resulting proteins were >95% pure as judged by SDS-PAGE. Pure proteins were concentrated to approximately 5 mg/mL, flash frozen in liquid nitrogen, and stored at −80 °C until use.

Small-angle X-ray scattering (SAXS). To inhibit aggregation, the Cys-free ESCRT-I complex was used for all SAXS experiments. Samples were dialyzed overnight at 4 °C against 50 mM Tris pH 7.4, 150 mM NaCl, 3 mM βME, 1 mM EDTA, 1% glycerol, and 0.18% ascorbic acid. Data were collected at concentrations of 0.5 to 5.0 $mg\,mL^{-1}$ at Stanford Synchrotron Radiation Lightsource beamline BL4-2. Data reduction and analysis were performed using the beamline software SAStool. The program AutoGNOM of the ATSAS suite (9) was used to generate $P(r)$ curves and to the determine maximum dimension (D_{max}) and radius of gyration Rg from the scattering intensity curve ($I(q)$ versus q) in an automatic, unbiased manner, and rounds of manual fitting in GNOM (10) were used to verify these values. Ab initio molecular envelopes were computed by the programs DAMMIN (11). Multiple iterations of DAMMIN were averaged using DAMAVER (12).

Labeling by MTSL and fluorescent dyes. To prepare MTSL-labeled ESCRT-I complex, the engineered double cysteine mutants in the background of the Cys-free construct were incubated overnight at 4 °C with 5 mM MTSL. Unreacted dye was removed by size exclusion chromatography on a Superdex 25 column (GE Healthcare). To prepare fluorescently labeled ESCRT-I complexes for single-molecule fluorescence experiments, double cysteine mutants were incubated overnight at 4 °C with a 5-fold molar excess of the appropriate dyes. The ratio of donor dye to acceptor dye was 1:3. Unreacted dyes were removed by size exclusion chromatography on a Superdex 25 column (GE Healthcare). The labeling efficiency was approximately one dye per cysteine residue as judged spectroscopically with a donor to acceptor ratio ~1:2. For bulk time-resolved fluorescence experiments, the

ESCRT-I complex was first incubated for 3 h at 4 °C at 1:0.2 molar ratio with donor dye. After the incubation, it was repurified using size exclusion chromatography at Superdex 25 column. At this stage only 8% of cysteine residues were labeled. Assuming a binomial distribution, virtually no doubly donor labeled protein was expected. Singly donor labeled ESCRT-I complex was used to measure the donor lifetime. To prepare doubly labeled ESCRT-I, donor-labeled protein was incubated with a 20-fold molar ratio of the cysteine reactive form of the acceptor dye and was used to measure the lifetime of donor fluorescence in the presence of acceptor. Labeling efficiency was approximately one dye per cysteine residue with 1:15 ratio of donor to acceptor as judged spectroscopically. Labeled proteins were concentrated to approximately 1 μM, flash frozen in liquid nitrogen, and stored at −80 °C until use. Cysteine reactive dyes Alexa488, Atto488, Alexa647, and Atto647 were used in this study.

DEER EPR spectroscopy. Pulse-EPR measurements were performed on 25–30 μL of sample loaded into quartz capillaries with 2.00 mm i.d. by 2.40 mm o.d. (Fiber Optic Center, Inc.). The protein concentration of double spin-labeled ESCRT-I mutants was in the 20- to 50-μM range in a 20 mM Tris pH = 7.4, 100 mM NaCl, and 10% wt/vol glycerol buffer. Prior to inserting into the instrument, the sample-containing capillaries were flash frozen in a dry ice/isopropanol bath. The DEER data were recorded at 80 K on a Bruker Elexsys-E580 spectrometer fitted with an ER4118X-MS3 split ring resonator (Bruker Biospin) at X-band frequency. Data were acquired using a four-pulse DEER sequence (13) with a 16 ns $\pi/2$ and two 32-ns π-observe pulses separated by a 28-ns π-pump pulse. The dipolar evolution times were typically 2.0–2.5 μs. The pump frequency was set to the center maximum of the nitroxide spectrum, and the observer frequency was set to the low field maximum, typically 65–70 MHz higher. The phase-corrected dipolar evolution data were processed assuming a 3D background and Fourier Transformed using the DeerAnalysis2009 package (14).

Time-resolved ensemble fluorescence measurements. Förster resonance energy transfer was observed between the atto488 and atto594 dyes covalently attached to Cys in the ESCRT-I protein complex. Fluorescence intensity decays were measured on a laser-based time-correlated single photon counting apparatus with multichannel plate photomultiplier detection described in detail previously (15) and analyzed by the maximum entropy method as discussed in detail in (16). Briefly, fluorescence intensity decays were acquired under the "magic angle" conditions where the measured intensity decay $I(t)$ is independent of a rotational diffusion of the chromophore and provides unbiased information about fluorescence lifetimes. The samples were placed in a thermostatic holder, and all experiments were performed at 22 °C in buffer containing 20 mM Tris-HCl (pH 7.4), 150 mM NaCl, and 1 mM EDTA. ESCRT-I concentration was 1 μM. Atto488 fluorescence was excited and collected at 310 nm and 520 nm, respectively. Fluorescence decays were processed using the singular value decomposition maximum entropy method, and mean lifetimes were calculated as described previously (16). The averaged efficiency of energy transfer E was calculated from the mean donor lifetime in the presence (τ_{DA}) and in the absence of acceptor (τ_D) according to $E = 1 - \tau_{DA}/\tau_D$.

The effective distance between the donor–acceptor pair R was calculated from $R = R_0(\frac{1}{E} - 1)^{1/6}$, where R_0 is the critical Förster distance, in this case equal to 5.7 nm.

Single-molecule experiments. Single-molecule FRET experiments were performed using a confocal microscope system (MicroTime200, PicoQuant). The donor fluorophore (Alexa Fluor 488) were excited by a linearly polarized dual mode (CW/pulsed) 485-nm diode laser (LDH-D-C-485, PicoQuant) at 30 μW through an oil-immersion objective (PlanApo, NA 1.4, ×100, Olympus). Donor and acceptor (Alexa Fluor 594) fluorescence, emitted from molecules freely diffusing through the illuminated volume, was collected by the same objective, divided into two channels, and focused through optical filters onto single-photon avalanche diodes (SPAD, PerkinElmer Optoelectronics SPCM-AQR-15). ESCRT-I (Vps28 Cys65-Cys151 and Vps28 Cys27—Vps37 Cys173) was diluted to 40 pM, which is sufficient to avoid having two molecules simultaneously in the illuminated volume (17), into a 20 mM Tris buffer (pH 7.4) with 100 mM NaCl and 3 mM β-mercaptoethanol. Bovine serum albumin was added (1 mg/mL) to prevent sticking of protein molecules to the glass coverslip. For steady-state polarization anisotropy measurements, the donor dye was excited with a laser in the pulsed mode at 20 MHz and fluorescence of the parallel and perpendicular polarizations was separated by a polarization cube. Donor and acceptor fluorescence of each polarization was further separated and collected by four SPADs. Other experimental details can be found in ref. 18.

Calculation of FRET efficiencies from model coordinates. Dyes attached to protein sites were previously simulated (19) and the distribution of distances between the Cys C_α atom and the active site in the dye was computed. We used the latter distance distribution to sample possible dye locations relative to the protein complex in the six selected conformations of ESCRT-I. Locations of the dye that overlapped with the proteins or with the other dye were excluded from the analysis. We assumed that all orientations of the donor and acceptor transition dipoles are equally probable. To calculate a FRET efficiency distribution from the model structures, the mean FRET efficiencies (Table S2) were calculated for each of the six selected structures. Using these six mean efficiencies and populations, the FRET efficiency histogram was constructed by the "recoloring" method described in refs. 1 and 2 in order to correctly account for shot noise. In this method, the colors (donor or acceptor) of the photons in each bin of the experimental data were removed. The cluster state was randomly assigned to the bin according to its relative population, and the photons were recolored using the apparent FRET efficiency of the assigned cluster state as the probability to observe an acceptor photon. Because this method uses exactly the same number of photons as that of the experimental data, it is the most rigorous way to account for the shot noise widths of each peak in the predicted histogram.

The mean FRET efficiency for dye pair (i,j) in ESCRT-I structure $k = 1,\ldots,n$ was calculated as $E_{k,(i,j)} = \langle[1 + (r_{\alpha\beta}/R_0)^6]^{-1}\rangle$, where R_0 is the Förster distance ($R_0 = 5.7$ nm and $R_0 = 5.4$ nm for the bulk and single-molecule FRET measurement, respectively) and the average is over all positions α and β of the dyes attached to sites i and j, respectively. For the label pair $(i,j) = (137,223)$, we calculated the ensemble average $E = \Sigma_k w_k E_k$. For the label pair $(i,j) = (65,151)$, single-molecule FRET efficiency histograms were calculated by the recoloring method (1, 2) to account for shot noise to compare directly to experiment.

Monte Carlo (MC) simulations. To create ESCRT-I structural ensembles, unbiased replica exchange Monte Carlo simulations were performed. After equilibration for 10^5 MC sweeps, 10^4 configurations were saved at regular intervals during a production run covering 10^7 MC sweeps. These configurations were grouped into clusters using the QT-clustering algorithm with DRMS as a metric (20) and a 1-nm cutoff. Structures at the cluster centers were used as representatives of their clusters in the ensemble refinement.

1. Gopich IV, Szabo A (2009) Decoding the pattern of photon colors in single-molecule FRET. *J Phys Chem B* 113:10965–10973.
2. Chung HS, et al. (2011) Extracting rate coefficients from single-molecule photon trajectories and FRET efficiency histograms for a fast-folding protein. *J Phys Chem A* 115:3642–3656.
3. Gopich IV, Nettels D, Schuler B, Szabo A (2009) Protein dynamics from single-molecule fluorescence intensity correlation functions. *J Chem Phys* 131:095102.
4. Gopich IV, Szabo A (2010) FRET efficiency distributions of multistate single molecules. *J Phys Chem B* 114:15521–15226.
5. Gopich I, Szabo A (2005) Theory of photon statistics in single-molecule Förster resonance energy transfer. *J Chem Phys* 122:014707.
6. Koshioka M, Sasaki K, Masuhara H (1995) Time-dependent fluorescence depolarization analysis in three-dimensional microspectroscopy. *Appl Spectrosc* 49:224–228.
7. Schaffer J, et al. (1999) Identification of single molecules in aqueous solution by time-resolved fluorescence anisotropy. *J Phys Chem A* 103:331–336.
8. Kostelansky MS, et al. (2007) Molecular architecture and functional model of the complete yeast ESCRT-I heterotetramer. *Cell* 129:485–498.
9. Petoukhov MV, Konarev PV, Kikhney AG, Svergun DI (2007) ATSAS 2.1—Towards automated and web-supported small-angle scattering data analysis. *J Appl Crystallogr* 40:S223–S228.
10. Svergun DI (1992) Determination of the regularization parameter in indirect-transform methods using perceptual criteria. *J Appl Crystallogr* 25:495–503.
11. Svergun DI (1999) Restoring low resolution structure of biological macromolecules from solution scattering using simulated annealing. *Biophys J* 76:2879–2886.
12. Volkov VV, Svergun DI (2003) Uniqueness of ab initio shape determination in small-angle scattering. *J Appl Crystallogr* 36:860–864.
13. Pannier M, et al. (2000) Dead-time free measurement of dipole-dipole interactions between electron spins. *J Magn Reson* 142:331–340.
14. Jeschke G, et al. (2006) DeerAnalysis2006—A comprehensive software package for analyzing pulsed ELDOR data. *Appl Magn Reson* 30:473–498.
15. Boura E, et al. (2007) Both the N-terminal loop and wing W2 of the forkhead domain of transcription factor FoxO4 are important for DNA binding. *J Biol Chem* 282:8265–8275.
16. Vecer J, Herman P (2010) Maximum entropy analysis of analytically simulated complex fluorescence decays. *J Fluoresc*, 10.1007/s10895-009-0589-1.
17. Gopich IV (2008) Concentration effects in "single-molecule" spectroscopy. *J Phys Chem B* 112:6214–6220.
18. Chung HS, Louis JM, Eaton WA (2009) Experimental determination of upper bound for transition path times in protein folding from single-molecule photon-by-photon trajectories. *Proc Natl Acad Sci USA* 106:11837–11844.
19. Merchant KA, et al. (2007) Characterizing the unfolded states of proteins using single-molecule FRET spectroscopy and molecular simulations. *Proc Natl Acad Sci USA* 104:1528–1533.
20. Rozycki B, Kim YC, Hummer G (2011) SAXS ensemble refinement of ESCRT-III CHMP3 conformational transitions. *Structure* 19:109–116.

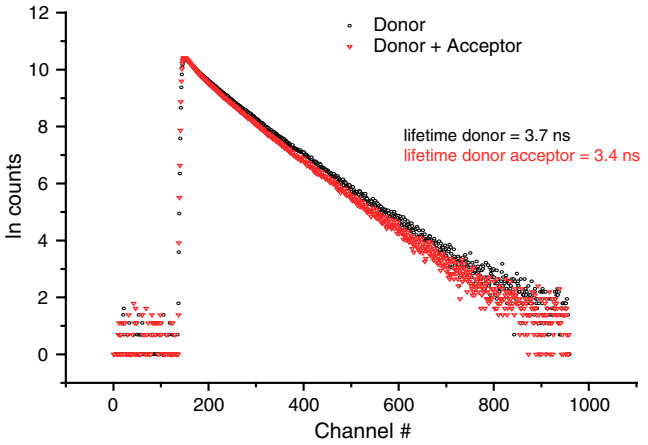

Fig. S1. Bulk FRET of the Vps23 Cys137—Cys223 pair.

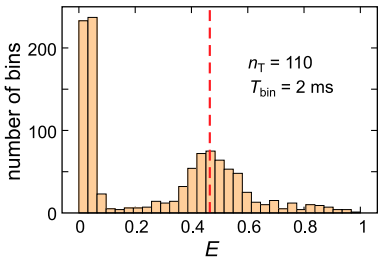

Fig. S2. ESCRT-I was assembled at 40 pM concentration. Single molecular FRET efficiency for the labeled Vps28 Cys27—Vps37 Cys173 pair is shown in light brown thick bars for $n_T = 110$ with a bin time (T_{bin}) of 2 ms, corrected as described in the legend to Fig. 5. The dashed red line shows the mean interdye distance calculated from the model structures.

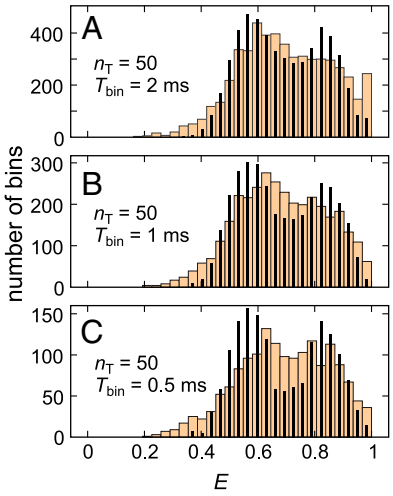

Fig. S3. The bin time dependence of the experimental FRET efficiency histogram (light brown thick bar) and the recolored histogram (black narrow bar) using maximum likelihood parameters (two FRET efficiencies and two rate coefficients) of the two-state kinetic model. The FRET efficiency of the recolored bin was γ-corrected in the same way as for the experimental values.

Table S1. Distance distribution parameters for ESCRT-I double mutants based on single Gaussian regularization of DEER data

Mutant pair	Mean distance Å	Standard deviation Å
27/173	52	7
12/223	28	16
108/256	26	20
65/151	23	17

Table S2. Relative populations and FRET efficiencies of 6 representative structural clusters found in the model structures

Cluster	Population	$\langle E \rangle$
1 (closed)	0.19	0.83
2 (open)	0.19	0.59
3 (closed)	0.23	0.90
4 (open)	0.10	0.70
5 (open)	0.21	0.60
6 (closed)	0.08	0.83

Table S3. Anisotropy of Alexa 488 and Alexa 594 attached to ESCRT-I

FRET efficiency range	<0.01	0.4–0.74	0.74–1
r_D	0.13	0.21	0.249
τ_D, ns	3.4	1.7	NA
τ_c, ns	1.6	1.9	1.0
r_A	NA	0.07	0.07
τ_A, ns	NA	4.2	3.9